CHAPTER 2

Experimental and computational methods

2.1 INTRODUCTION

This chapter provides a comprehensive overview of experimental and computational methodologies employed in this thesis. It includes a detailed discussion of the various sophisticated instruments used in the experimental work, the characterization techniques, and their corresponding sample preparation methods. Additionally, a table listing all the chemicals utilized in the study is presented for clarity.

The experimental conditions for photocatalytic H_2O_2 production, along with the methods used for its determination, are also discussed in this chapter.

2.2 CHEMICALS

All chemicals used in the synthesis were of analytical grade and used without further purification. The chemicals utilized in this thesis are listed in Table 2.1. Double-distilled water (DW) was utilized to prepare the sample and evaluate its photocatalytic activity.

Table 2.1 Chemicals used for the experiments in this thesis work

Chemical name	Formula	Molecular mass (g/mol)	Company
Nickel nitrate hexahydrate	$Ni(NO_3)_2.6H_2O$	290.79	Merck
Cobalt (II) acetate	$Co(CH_3CO_2)_2 \cdot 4H_2O$	249.08	Merck
Sodium tungstate dehydrate	$Na_2WO_4 \cdot 2H_2O$	293.82	Merck
Iron (III) nitrate nonahydrate	$Fe(NO_3)_2 \cdot 9H_2O$	341.9	Merck
Copper nitrate hexahydrate	$Cu(NO_3)_2 \cdot 6H_2O$	295.65	Merck
Sodium borohydride	$NaBH_4$	37.83	Merck

Sodium hydroxide	NaOH	40	Merck
Ammonium molybdate tetrahydrate	$(NH_4)_6Mo_7O_{24}\cdot 4H_2O$	1235.86	Wako
Indium chloride tetrahydrate	$InCl_3\cdot 4H_2O$	293.24	Wako
Ethylenediaminetetraacetic Acid Disodium	$C_{10}H_{14}N_2Na_2O_8$	336.21	Merck
Manganese chloride tetrahydrate	$MnCl_2\cdot 4H_2O$	197.90	Wako
Nitroblue tetrazolium chloride	$C_{40}H_{30}Cl_2N_{10}O_6$	817.64	Merck
Thiourea	$CS(NH_2)_2$	76.12	Wako
Silver nitrate	$AgNO_3$	169.87	Merck
Potassium iodide	KI	166.00	Merck, Wako
Isopropanol	C_3H_8O	60.10	Merck
Ethanol	C_2H_5OH	46	Merck
p-Benzoquinone (p-BQ)	$C_6H_4O_2$	108.09	Sigma Aldrich
Sulphuric Acid	H_2SO_4	98	Merck
Hydrochloric Acid	HCl	36.46	Merck
Starch	--	--	Merck
Ammonia	NH_3	17	Merck
Tetracycline	$C_{22}H_{24}N_2O_8$	444.4	Sigma Aldrich

2.3 EXPERIMENTAL PART

2.3.1 Sample preparation

The samples (photocatalyst nanoparticles) were prepared by stepwise co-precipitation, hydrothermal, and liquid-mediated exfoliation methods. Hydrothermal syntheses were carried out in a Teflon-lined stainless-steel autoclave. Detailed descriptions of the photocatalyst preparation methods are provided in the *Sample Preparation* sections of Chapters 3, 4, 5, 6, and 7.

2.3.2 Material Characterizations

This section outlines the techniques used to characterize the synthesized photocatalysts. X-ray diffraction (XRD) was employed to determine the crystalline structure and identify the phases present in the nanomaterials. Transmission electron microscopy (TEM) and scanning electron microscopy (SEM) provided detailed images of the nanoparticles, including their size, shape, and overall morphology. High-resolution TEM (HR-TEM) imaging was used to capture crystalline fringes, and the interplanar d-spacing calculated from these fringes confirmed the presence of specific phases. Additionally, energy-dispersive X-ray spectroscopy (EDX) mapping, performed using SEM and TEM, provided insights into the elemental distribution and confirmed the stoichiometry of each element within the photocatalysts. UV-visible diffuse reflectance spectroscopy (UV-DRS) was employed to measure the reflectance data of the synthesized samples. The bandgap of the photocatalysts was determined from Tauc plots derived from the UV-DRS data. Photoluminescence (PL) analysis was performed to evaluate the fluorescence intensities of the solid samples, providing insights into their electronic properties and the efficiency of charge separation within the photocatalytic systems. X-ray photoelectron spectroscopy (XPS) was utilized to identify the elemental composition, oxidation states, and electronic environments within the materials. It also provided

information on the binding energies of the constituent elements. UV-visible spectroscopy was used to measure the absorbance of reaction mixtures during photocatalytic experiments. Contact Angle measurements were used to assess the hydrophilic characteristics of photocatalysts. A vibrating sample magnetometer (Microsense EZ9 VSM) was used to examine the magnetic characteristics of the synthesized samples.

2.3.2.1 Powder X-ray diffraction (PXRD)

Powder X-ray diffraction (XRD) is a key technique for characterizing crystalline materials and providing information on phase identification, crystallinity, and structural properties [73]. It is a non-destructive method, allowing solid samples to be fully recovered after analysis. When a collimated X-ray beam strikes the sample, it is diffracted in specific directions corresponding to the crystallographic planes. This diffraction follows Bragg's law, expressed as:

$$n\lambda = 2d\ sin\ \theta \dots\dots\dots\dots\dots\dots\dots (2.1)$$

where λ is the X-ray wavelength, n is the order of diffraction, d is the interplanar spacing, and 2θ is the angle between the incident and diffracted beams.

Powder XRD patterns were recorded using a Rigaku Miniflex 600 Desktop instrument (RIGAKU Corporation, Japan) equipped with a Cu Kα radiation source (λ = 1.54056 Å). Data collection was performed at a scan rate of 5° per minute with a step size of 0.01° over a 2θ range of 5°–80°. In Chapter 7, high-resolution XRD (HR-XRD) was conducted using Cu Kα radiation on an Ultima IV (Rigaku, Japan) with a step size of 0.01° and a scan rate of 1°/min. The obtained diffraction patterns were matched with standard patterns from the JCPDS database to identify the crystalline phases. For XRD analysis, the samples (agglomerated nanoparticles) were finely ground to achieve a uniform particle size,

ensuring accurate diffraction results. The ground powder was evenly spread onto an XRD sample holder, typically made of glass or aluminum. Care was taken to minimize surface irregularities and ensure a flat, uniform sample surface for accurate diffraction measurements. The prepared sample was then mounted in the XRD instrument for phase identification and crystallographic analysis.

2.3.2.2 Scanning electron microscope (SEM) & Energy-Dispersive X-ray Spectroscopy (EDX)

SEM is an advanced imaging technique that scans a sample's surface with a focused electron beam to generate high-resolution images [74]. The interaction between electrons and the sample produces signals that reveal critical details about morphology, size, and elemental distribution, making it invaluable for nanoparticle analysis. Additionally, EDX mapping enhances SEM by identifying and spatially mapping elements within the sample, confirming their successful incorporation and uniform distribution.

In this thesis work, the SEM images and elemental mapping were captured on the Nova Nano SEM 450 (FEI Company of USA (SEA) PTE, LTD) instrument. In Chapter 7, the morphology and elemental mapping were analyzed using an SEM (JEOL, JSM-6010LA). For the SEM measurements, the samples were prepared following the standard sample protocol for powder nanoparticle samples. A small amount of the nanoparticle powder was evenly spread onto a conductive carbon adhesive tape mounted on an SEM stub. To prevent contamination and ensure a clean imaging surface, excess particles were gently removed using an air duster. If the nanoparticles were non-conductive, a thin coating of gold or platinum was applied to enhance conductivity. Finally, the prepared stub was directly placed into the SEM instrument for analysis.

2.3.2.3 Transmission electron microscope (TEM)

TEM is a crucial technique for analyzing nanoparticles, offering insights into their structural and morphological properties at the nanoscale. It provides high-resolution images that reveal the size, shape, and distribution of nanoparticles with exceptional clarity [75]. TEM also enables the identification of crystalline phases and lattice arrangements. Techniques such as High-Resolution TEM (HRTEM) and Selected Area Electron Diffraction (SAED) further enhance its capability by providing detailed crystallographic information, aiding in understanding the structure-property relationships of nanoparticles. This method utilizes a heated tungsten filament within the electron gun to generate electrons, which are then focused onto the specimen using condenser lenses. Upon interacting with the specimen, the electrons undergo scattering and are subsequently directed by magnetic lenses to produce a magnified and well-defined image. As the electrons pass through a fluorescent screen, a polychromatic image is formed. Denser regions of the specimen appear darker because they scatter more electrons, reducing the number that reaches the screen for visualization. In contrast, thinner or more transparent regions appear brighter due to reduced electron scattering.

To prepare the TEM specimen, 1 mg of the nanoparticle sample was dispersed in 1 mL of ethanol using ultrasonication to ensure a uniform suspension. A 1 μL droplet of this well-dispersed suspension was then carefully deposited onto a 400-mesh nickel/copper grid (Ted Pella, Inc.). The grid was allowed to air dry completely before proceeding with the TEM analysis. The imaging was performed using a Tecnai G2 20 TWIN (EDAX Inc.) and a JEOL-3100 TEM instrument (used specifically for Chapter 7), both operated at an accelerating voltage of 200 kV. To analyze the TEM images, the average particle sizes and lattice fringe d-spacing were calculated using Image J software and Digital Micrograph.

2.3.2.4 X-ray photoelectron spectroscopy (XPS)

X-ray Photoelectron Spectroscopy (XPS) is a powerful quantitative technique used to analyze the chemical composition and oxidation states of elements in a material [76]. When X-rays are directed at the sample, they interact with the atoms, causing the photoelectric effect. This process ejects electrons from the material's surface, and these ejected electrons have specific kinetic energies. By measuring the kinetic energies of these electrons with a detector, the binding energies of the electrons can be calculated. Each element and its particular oxidation state have a characteristic binding energy, allowing for the precise identification of the chemical states present in the material. XPS can also reveal the presence of surface contaminants, oxidation, and any changes in the chemical environment, offering valuable insights into the structure-property relationships of nanoparticles. In this present work, the XPS measurements were performed using the K-ALPHA XPS instrument (Thermo Fisher Scientific). For the XPS measurements, the samples were prepared by dispersing a small amount of nanoparticles in ethanol using an ultrasonication bath. The resulting dispersion was then dropped onto a small, square-shaped glass slide. The glass slide was dried in a hot air oven at 60°C. This process was repeated several times until the glass slide was fully covered with a thin layer of the sample. The prepared glass slide with the thin film of the sample was then subjected to XPS measurements. For the analysis of the XPS data, CasaXPS and XPSPeak 4.1 software were used for data fitting and interpretation.

2.3.2.5 UV-visible diffuse reflectance spectroscopy (UV-DRS)

The UV-DRS is a widely used technique for evaluating the optical properties and energy band gap of photocatalysts. It allows for the measurement of light absorption across the ultraviolet (UV) and visible regions of the spectrum, providing insights into the

electronic structure and band gap of photocatalytic materials. By analyzing the diffuse reflectance spectra, the absorption edge and the onset of the photocatalyst's optical absorption can be determined, which is crucial for understanding its photocatalytic activity. The measurements were conducted using a UV-2600 spectrophotometer, and specifically, the SolidSpec-3700 DUV (Shimadzu, Japan) was used in Chapter 7, both equipped with an integrating sphere assembly. $BaSO_4$ was used as the reference for reflectance. For UV-DRS measurements, the as-prepared photocatalyst nanoparticles were directly placed into the disc-shaped sample holder, which was equipped with a quartz base. The sample holder was then inserted into the UV-DRS spectrophotometer, and measurements were performed over the desired wavelength range.

The generated reflectance data were then converted into absorbance values using the Kubelka-Munk method [77]. These absorbance values were subsequently used to generate Tauc plots, as shown by the following relation (Equation 2.2).

$$(\alpha h\nu)^{\frac{1}{n}} = A(h\nu - E_g) \quad \ldots\ldots\ldots\ldots\ldots\ldots (2.2)$$

Here, α represents the molar absorption coefficient, and E_g and ν denote the material's bandgap and light frequency, respectively. The optical bandgap (E_g) of the photocatalyst can be determined from the x-axis intercept of the tangent to the linear portion of the plot of $(\alpha h\nu)^{1/n}$ vs. $h\nu$. The value of n determines the nature of the optical bandgap: for a direct bandgap, n equals 1/2, while for an indirect bandgap, n equals 2.

2.3.2.6 UV-Visible spectroscopy

UV-visible absorption spectroscopy is a powerful analytical technique used to measure the absorbance of light in the ultraviolet (UV) and visible regions of the

electromagnetic spectrum. The technique involves passing light of varying wavelengths through a sample and recording the intensity of the transmitted light to determine the absorbance. When light interacts with a sample, it can be absorbed, transmitted, or reflected. During absorption, electrons in the molecule are photo-excited, leading to electronic transitions such as $n \rightarrow \pi^*$, $\pi \rightarrow \pi^*$, and $n \rightarrow \sigma^*$, where n represents a non-bonding orbital, π denotes a bonding π-orbital, π^* is an anti-bonding π-orbital, and σ^* is an anti-bonding σ-orbital. The resulting absorbance spectrum, typically plotted as absorbance versus wavelength, can be used to identify functional groups and analyze concentrations using the Beer-Lambert law [78]. The UV-visible spectra of the samples were recorded using an Agilent Cary 60 spectrophotometer. For analysis, a diluted sample solution was placed in a 1 cm path-length quartz cuvette and positioned in the spectrometer's sample holder. The solvent used in the sample preparation served as the baseline for correction.

2.3.2.7 Vibrating sample magnetometer

A VSM is a precise instrument used to measure the magnetic properties of nanomaterials at room temperature. In this technique, a sample is magnetized by an external magnetic field and mechanically vibrated at a fixed frequency. The vibration induces an alternating magnetic flux, which is detected by pickup coils to determine the magnetization of the sample [79]. VSM allows for the characterization of key magnetic parameters such as saturation magnetization, coercivity, and remanence. The magnetic measurements were performed using a Microsense EZ9 VSM instrument. An appropriate amount of the nanoparticle sample was carefully loaded into the VSM sample holder, which was then securely positioned within the instrument for measurement.

2.3.2.8 Contact angle measurements

To investigate the influence of surface properties on photocatalytic H_2O_2 production, contact angle measurements were conducted to evaluate the hydrophilicity of the nanoparticles. This analysis provides critical insight into how surface wettability affects the interaction between the catalyst and the aqueous phase, thereby influencing catalytic performance [80]. Model, CA, XP were used as the contact angle instruments. For contact angle measurements, a thin pellet of the nanoparticles was prepared by compressing the nanopowder sample using a hydraulic press. The resulting dense and smooth pellet surface was used for contact angle analysis, ensuring a consistent and uniform substrate to evaluate the wettability and hydrophilic properties of the nanoparticles.

2.3.3 Electrochemical measurement tests

The electrochemical studies, specifically Mott-Schottky (MS) and electrochemical impedance spectroscopy (EIS), were conducted using a standard three-electrode setup in an electrochemical workstation (CHI-660E) and Metrohm Autolab. A carbon electrode was employed as the counter electrode, an Ag/AgCl electrode served as the reference electrode, and carbon paper or *fluorine-doped tin oxide* (FTO) was used as the working electrode. The working electrode was prepared as follows: 2.5 mg of the photocatalyst was dispersed in 250 µL of a deionized water/ethanol mixture (1:1 ratio) via 30 minutes of ultrasonic bath sonication. Then, 10 µL of Nafion reagent was added, and the mixture was sonicated for an additional 30 minutes. Afterward, 40 µL of the resulting suspension was evenly applied to the carbon paper within a 0.25 cm^2 area and allowed to dry at room temperature to form the working electrode. Note that 0.5M Na_2SO_4 electrolyte was used for the above measurements (the pH value of the electrolyte was around 7). The VB and the CB band potentials of the p-type and n-type photocatalysts were determined by fitting their MS plots [81]. The potentials obtained against Ag/AgCl (reference electrode) were then converted to

the normal hydrogen electrode (NHE) scale using Equation 2.3 [82]. For the photocurrent measurement, the photo-electrode was fabricated using the same above-mentioned protocol. A solar simulator was used as the light source to illuminate the electrode.

$$V_{NHE} = V_{(Ag/AgCl)} + 0.059 * pH + 0.197 \ldots\ldots\ldots\ldots\ldots\ldots \quad (2.3)$$

2.3.4 Photocatalytic H_2O_2 performance measurement and their detection

The photocatalytic experiments were performed under visible light irradiation using a 14W Philips cool white LED bulb as the light source. In Chapter 7, a solar simulator equipped with a xenon lamp was utilized for photocatalytic measurements. For photocatalytic experiments, the desired amount of nanoparticles (photocatalyst) was dispersed in an appropriate volume of deionized distilled water (DW) using an ultrasonic bath. Oxygen (O_2) was then bubbled through the prepared suspension, which was subsequently exposed to visible light irradiation. The detailed procedures for the photocatalytic experiments are provided in Chapters 3, 4, 5, 6, and 7. The amount of H_2O_2 produced after the photocatalytic reaction was quantified using two methods: the standard $KMnO_4$ titration method and the iodometric method. Notably, the $KMnO_4$ titration method was applied exclusively in Chapter 3, while the iodometric method was used in all other chapters.

2.3.4.1 Experimental details for H_2O_2 determination

The H_2O_2 amount produced (after photocatalyst separation) was determined by a redox titration of 2 ml of the sample solution with standard acidified (using 1M H_2SO_4) 0.2 mM (aqueous) $KMnO_4$ solution. The solution turning pink indicated the endpoint of the (H_2O_2 – $KMnO_4$) titration. Additionally, an iodometric method using absorbance spectroscopy was also employed to verify the H_2O_2 production quantitatively. At regular

intervals during the photocatalytic reaction, after removing the photocatalyst, a 2 mL aliquot was extracted from the reaction mixture. To this aliquot, 2 mL of 0.1 M KI and 50 µL of 0.01 M ($(NH_4)_6Mo_7O_{24}\cdot 4H_2O$) were added and thoroughly mixed. The reaction mixture was then kept in the dark for 20 minutes to ensure a complete reaction before absorbance measurements were taken. In this process, KI is oxidized by H_2O_2, releasing I_2, which then reacts with excess I^- (from KI) to form the yellow-colored triiodide anion (I_3^-) through the reaction: $H_2O_2 + 3I^- + 2H^+ \rightarrow I_3^-$. The amount of I_3^- generated is directly proportional to the concentration of H_2O_2 present in the sample. Finally, the absorbance of the resulting solution was measured using UV–vis spectroscopy, showing a characteristic intense absorption peak around 352 nm. The concentration of H_2O_2 formed was calculated by interpolating the absorbance intensity in a calibration plot prepared previously using known H_2O_2 concentrations (Figure 2.1).

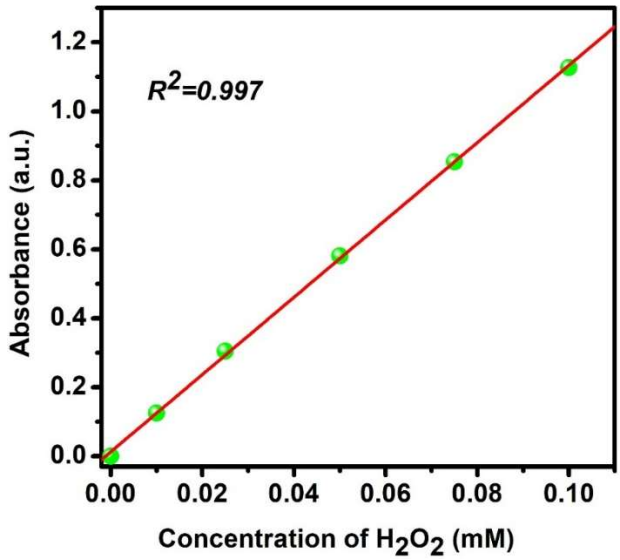

Figure 2.1. The calibration of H_2O_2 at different known concentrations

2.3.4.2 Experimental details of superoxide detection by NBT (Nitroblue Tetrazolium) test

The NBT assay was used to spectrophotometrically quantify the production of superoxide radicals in the aqueous solution of the desired photocatalyst [83]. Experiments were conducted under an oxygen flow. In a typical procedure, the appropriate amount of desired photocatalyst nanoparticles was dispersed in 20 mL of a 2.5×10^{-5} mol/L NBT solution and irradiated with a cool white LED or solar simulator (Chapter 7). After the reaction, the photocatalyst was separated magnetically or centrifuged at different time intervals, and 2 mL of the supernatant was analyzed using a UV-Vis spectrophotometer to measure the superoxide formation.

2.4 COMPUTATIONAL PART

2.4.1 Molecular dynamics simulation

This section provides a concise overview of the fundamental aspects of classical MD simulations. MD simulation is a powerful computational technique used to analyze and predict the behavior of systems at the atomic and molecular levels. It serves as a valuable tool for gaining insights that are often difficult or impossible to obtain through experimental methods. By simulating the movement of atoms and molecules over time, MD simulations provide a detailed understanding of various physical and chemical properties [84]. One of the key advantages of MD simulations is their ability to capture dynamic information about atomic interactions, which helps in predicting both thermodynamic and kinetic properties [85]. Thermodynamic properties include parameters such as temperature, pressure, and free energy, which govern the stability and phase behavior of a system. Meanwhile, kinetic properties, such as reaction rates and diffusion coefficients, describe how fast molecules move and interact within a given environment. Classical MD simulations operate on the principles of classical mechanics, which means they do not account for quantum effects and are used for modeling molecular systems where chemical bonds remain intact. These

simulations rely on solving Newton's equations of motion to track the trajectories of atoms and molecules over time [85]. By integrating these equations, MD simulations can map out how a system evolves within a multi-dimensional phase space, which consists of all possible positions and momenta of the particles involved.

In this thesis, MD simulations were performed to examine the adsorption and interaction behavior of O_2 and H_2O molecules on heterostructure photocatalysts. When developing or designing a heterostructure photocatalyst for H_2O_2 formation, researchers often face the challenge of selecting which semiconductor component is better suited for oxygen adsorption and which one favors interaction with water. Understanding the interaction between photocatalyst components and oxygen and water molecules is essential before conducting blind experiments. In this context, the MD Simulation Method is a powerful tool for molecular-level studies. Several experimental reports are available on photocatalytic H_2O_2 production. However, there is still limited understanding of the underlying mechanism governing photocatalytic H_2O_2 generation. In the present work, large-scale classical MD simulations were employed to investigate the oxygen and water adsorption affinities of the respective semiconductor components.

The first step in MD simulation is setting up the initial model by defining parameters such as temperature, molecules, density, simulation time, and time step [49]. The initial system configuration should have a finite probability of occurrence under the given temperature and ensemble conditions. Prior to the simulation, energy minimization is essential to eliminate structural strains or unfavorable interactions, preventing numerical instabilities and ensuring a physically stable starting structure. Techniques like steepest descent or conjugate gradient minimization are commonly used for this purpose. Once

equilibrium is achieved, the system stabilizes, with macroscopic properties like temperature, pressure, and energy fluctuating around consistent averages.

All simulations conducted in Chapters 3, 4, and 5 of this thesis employ periodic boundary conditions with appropriate cut-offs. In this approach, the central system (or simulation box) is surrounded by identical replica cells, ensuring continuity. Molecular movements within the central system are mirrored in all surrounding replicas. Consequently, when a molecule exits through the right boundary of the central cell, another molecule enters from the corresponding mirror system on the left. To obtain valid ensemble averages, simulations are run for sufficiently long durations. The system is first equilibrated over an extended period, followed by the production run, during which data is collected to compute ensemble-average properties [86]. Analysis of production run data provides valuable insights into the structural characteristics of the system, including radial distribution functions (RDF) and adsorption properties (such as density profiles, adsorption energies, and hydrogen bonding).

2.4.2 Water Models

This thesis employs MD simulations to investigate interfacial phenomena, specifically the adsorption of reactant molecules in an aqueous environment. Given the crucial role of water in these simulations, selecting an accurate water model is essential for obtaining reliable MD results. Numerous water models exist, each designed to replicate specific structural or thermodynamic properties of actual water in condensed phases. The most widely used water models belong to the first group, particularly the simple three-site ones, such as the SPC or TIP3P models [87]. In this work, two different water models were utilized for simulations. Chapters 3 and 4 employed the TIP3P (Transferable Intermolecular

Potential 3-Point) model, while Chapter 5 utilized the Simple Point Charge (SPC) water model.

2.4.3 Ensembles

An ensemble is a collection of microstates (configurations) that a system can explore under a defined set of thermodynamic constraints. Commonly used ensembles include NVE (constant number of particles (N), volume (V), and energy (E)), NVT (constant number of particles (N), volume (V), and temperature (T)) [88] and NPT (constant number of particles (N), pressure (P), and temperature (T)) [89]. Each ensemble represents distinct thermodynamic conditions and is selected based on the specific requirements of the simulation. MD simulations of the adsorption properties discussed in Chapters 3, 4, and 5 of this thesis were performed using the NVT ensemble. In the NVT ensemble, "N," "V," and "T" remain fixed. While the system exchanges energy with its surroundings, the total number of particles and volume remains unchanged. In canonical (NVT) ensembles, the system is not thermally isolated, leading to fluctuations in its total energy. This characteristic is controlled in the simulations conducted for this thesis using the Nosé-Hoover thermostat.

2.4.4 Force Field

The selection of an appropriate force field is a fundamental and crucial step in MD simulations, as it determines the accuracy of the system's energy calculations and dynamics [90]. A force field defines the potential energy of a system using mathematical expressions that describe atomic interactions. The total potential energy in a force field is generally divided into two main components: bonded and non-bonded interactions. Bonded energy contributions include (a) atomic stretching, (b) bond angle between atoms, and (c) dihedral

angle rotations. Non-bonded interactions comprise van der Waals forces, represented by the Lennard–Jones potential, and (e) electrostatic interactions, governed by Coulomb's law. In Chapters 3, 4, and 5 of this thesis, the Dreiding force field is used to describe interatomic interactions during MD simulations. Unlike many force fields designed for specific systems, the Dreiding force field prioritizes broad applicability by employing a set of simple and transferable parameters that encompass nearly all elements in the periodic table.

2.4.5 Software utilized in MD simulation

In this thesis, molecular modeling and result analysis were conducted using MAPS (Materials and Process Simulation) software, version 4.1.1, developed by SCIENOMICS. MD simulations and calculations were performed using LAMMPS (Large-scale Atomic/Molecular Massively Parallel Simulator) on the PARAM SHIVAY supercomputer at IIT (BHU), Varanasi.